
Development and description of a Raman LIDAR

Alicia LÓPEZ ORAMAS

15th July, 2010

Supervised by Dr. Oscar BLANCH

Contents

1	Introduction	5
2	The Raman LIDAR Technique	9
3	The IFAE LIDAR	13
4	Reflectivity	21
4.1	Superficial Reflectivity	21
4.2	Focused Reflectivity	23
4.2.1	Methodology	24
4.2.2	Results	28
5	Point Spread Function	33
6	Summary	37

Chapter 1

Introduction

Imaging Air Cherenkov Telescopes (IACT) detect and examine Cherenkov light emitted by extended air showers that are produced by gamma rays when they enter into the atmosphere. The gamma ray interacts with the atmosphere atoms producing a cascade of particles traveling faster than light. Cherenkov light, whose emission peak is around 350nm, produced by these secondary particles is collected by a large mirror and focused to an ultrafast highly pixelized camera. The light from a single extended shower lasts for few ns and forms an image of that cascade in the camera. The former allows us to discriminate showers from the diffuse night sky background and the latter provides the power to discriminate showers produced by gamma rays from those generated by other particles like hadrons, which are a physical background. Moreover, the image recorded by the camera also let us reconstruct the energy and the incoming direction of the initial gamma ray. This enables Cherenkov telescopes to study high energy gamma radiation in the GeV-TeV range.

Very high energy gamma ray astrophysics has reached its golden age in the last five years thanks, mainly, to the development of new observatories as MAGIC and HESS, known as third generation of Cherenkov telescopes. These success have favored the wish in the scientific community to carry out and create the next generation of telescopes as the CTA project, which will lead to an observatory with numerous and better instruments of this kind.

MAGIC ¹(Major Atmospheric Gamma-Ray Imaging Cherenkov) is a high gamma ray observatory placed at El Roque de los Muchachos (La Palma, Canary Islands, Spain) which has the two biggest and most advanced Cherenkov telescopes over the world, besides from owning the ground instrument with the lowest trigger threshold. It's made up of two telescopes, MAGIC-I and MAGIC-II, this last one on is in its first year of operation and it was created to extend the program already started by its analogous. The critical points to achieve this objective are the reduction of the thresh-

¹<http://wwwmagic.mppmu.mpg.de/>

old and the better sensitivity thanks to stereoscopic observation, which also will allow us to locate with more precision the source of gamma rays. All of these pieces together will enable, for example, the detector to be more sensitive to remote AGNs, extragalactic objects that can contribute with important information to fundamental physics fields such a quantum gravity and cosmology.

On the other hand, CTA² (Cherenkov Telescope Array) is a project that pretends to improve current instruments sensitivity in an order of magnitude and increase the energy range. It's thought to be taking its first data in five years, approximately. It will consist of two observatories: one on the southern hemisphere, focused on the high energy range (100GeV-100TeV) in order to study galactic sources and the Milky Way center; and a northern observatory equipped with low energy instrumentation (10GeV-1TeV) which will be mainly dedicated to extragalactic sources.

One possible improvement could be achieved by the use of a Raman LIDAR, a device designed to monitor the atmosphere transmission probability, a key fact in a large observatory as CTA would be. On the one hand, the knowledge of the vertical distribution of aerosols would boost systematics errors due to atmospheric quality changes. On the other hand, the knowledge at any moment of the atmosphere transmitivity would allow CTA to correct data taken without perfect weather conditions. Currently, Cherenkov telescopes simply discard this date, which may account for more than 30% of the duty cycle. The economical effort and concept of CTA make this approach unreasonable and LIDARs may be the solution. Utilization of an instrument of this kind would be a great step in this field because no other Cherenkov telescope works at present with a Raman LIDAR.

Because of all this necessities and requests, this project has the aim of understanding the start up of a Raman LIDAR and its limitations, as well as the development and characterization of the LIDAR which is being built at IFAE for CTA observatory. Likewise, it pretends to study what the optimum point of operation is for the required application. In order to carry out this characterization of the system, measurements of the mirror's differential and focused reflectivity and Point Spread Function (PSF) determination will be done.

²<http://www.mpi-hd.mpg.de/hfm/CTA/>

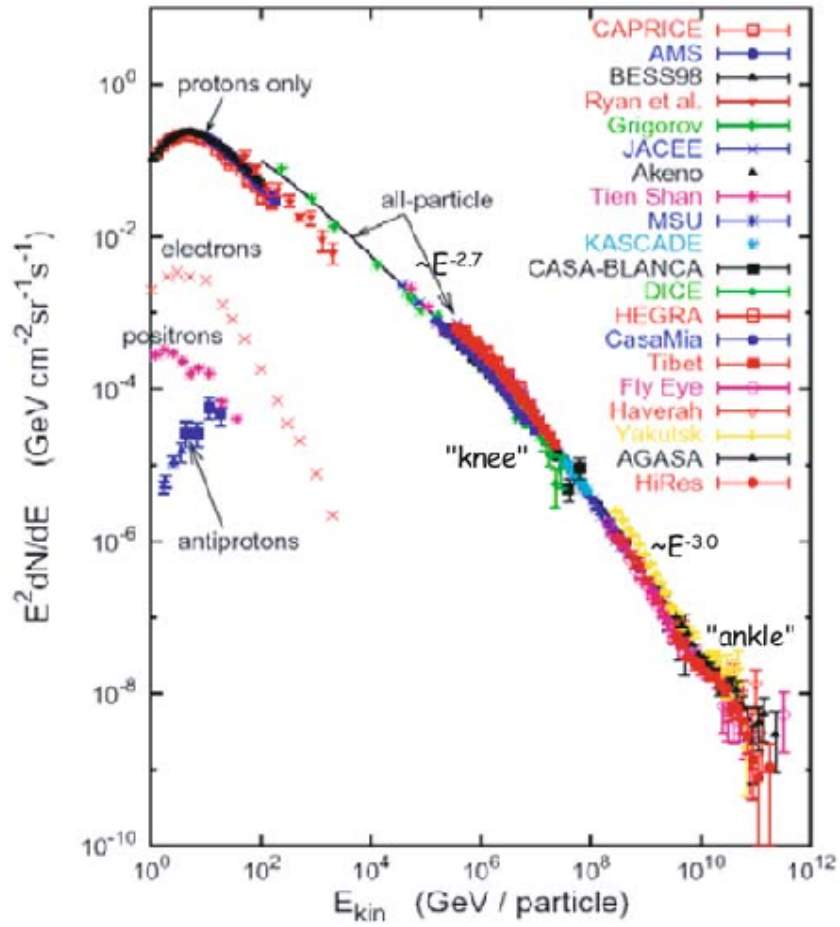


Figure 1.1: Cosmic Ray spectrum obtained by different experiments. Significant features as the knee and the ankle are indicated. Image taken from [1]

Chapter 2

The Raman LIDAR Technique

Raman spectroscopy provide information of chemical and structural composition of the material or element that we pretend to analyze as, in this case, the terrestrial atmosphere would be.

This technique is based in the analysis of the backscattered light from the molecules when a monochromatic beam characterized with a frequency ν is thrown over them.

Part of this light would be elastically dispersed with the same frequency it was received, producing the well-known Rayleigh Scattering, which doesn't give any information about the elements in the atmosphere, to be precise. Nevertheless, a small fraction is scattered in an inelastic way, thanks to the Raman Scattering, which is rotor-vibrational and non-elastic, so the backscattered radiation would suffer a shift in its wavelength, characteristic of the stationary states of each molecule, what allows to identify the chemical composition of the sample. These shifts are independent of the incoming radiation and are characteristic of the physical state and the chemical nature. Moreover, the importance of using Raman LIDAR technique is not only the knowledge of the elements in the atmosphere but also to break the degeneration we could measure to obtain the vertical distribution of these aerosols, as it would be explained below.

Raman Scattering is associated to a variation in the vibrational and rotational states of molecules and, so, it depends on energy changes. This effect takes place when the light collides with a molecule and interacts with its electron cloud. When the photon interacts with the molecule, this last one it is transiently elevated from its ground state to a virtual vibrational or rotational energy state. This state is fastly abandoned to fall into a permitted level different from the initial one and, during this process, it emits a photon whose frequency, ν_R , is shifted from the initial monochromatic beam frequency, ν . This shift in the emitted photon frequency depends on the dif-

ference in energy between this two levels and could be bigger or smaller than the original one, depending if the energy transfer is done from the molecule to the photon or vice versa: if the final state is more energetic, then the emitted photon will be shifted to a lower frequency so the total energy of the system remains balanced, process known as *Stokes shift*; if it goes to a more energetic state it is called *Anti-Stokes shift*. This process is illustrated in Figure 2.1³.

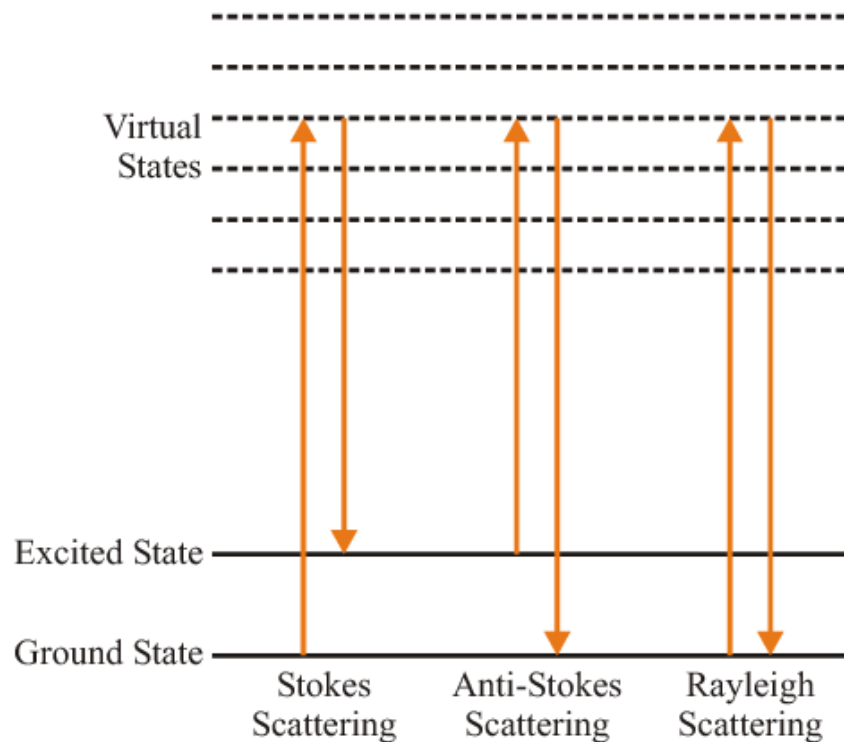


Figure 2.1: Energy diagram of Rayleigh and Raman Scattering, pointing out the Stokes and Anti-Stokes possibilities

As Cherenkov astronomy uses the atmosphere as a calorimeter, atmospheric quality has to be taken into account. The study of Rayleigh and Raman Scattering provides a tool to characterize the atmosphere.

Main components of a Raman LIDAR are a laser, a reflecting surface and a detector element. It is a radar optical analogous and studies the atmosphere through the sending of short light pulses with a laser. The laser and the collecting surface will point at the same direction so the light emitted by the first one and reflected by molecules in the atmosphere will be caught and concentrated in the focus by the second one. The collected light

³Image taken from: http://www.hyperdeath.co.uk/silicon_photonics/chapter6.php

is then guided to the detector. There, the interesting wavelengths are selected by means of filters, beam splitters and dichroic mirrors. Each Raman wavelength is sent to a different photodetector, which is used to record the amount of light which is reaching the LIDAR as a function of time. Time can be easily converted to height by computing the light path. That would be the experimental input to finally get the optical depth τ through equation 2.2.

As the laser is a known source, we could study how the radiation which reach us scatter by molecules in the atmosphere is and how optical depth varies with the altitude. We could also determine the vertical distribution of aerosols and clouds, elements which absorb part of the light coming from fluorescences. That would allow us to convert the amount of Cherenkov light measured by the telescope to that really produced in the atmosphere.

The amount of light backscattered from molecules depends on the attenuation suffered by radiation since it was emitted and also on the backscatter cross section from the point of scattering. This last one is dependent on the composition and shape of aerosols, so it could vary with them. The backscattered signal is described by LIDAR equation [4]:

$$P(r, \lambda) = P_0 \frac{ct_0}{2} \beta(r, \lambda) \frac{A}{r^2} e^{-2\tau(r, \lambda)} \quad (2.1)$$

where $P(r, \lambda)$ is the radiation scattered by molecules, P_0 is the initial radiation emitted by the laser, c is the speed of light, t_0 is the time of the transmitted pulse, $\beta(r, \lambda)$ is backscatter coefficient, where r is the distance to the molecule and λ is the wavelength. $\tau(r, \lambda)$ represents the optical depth, which could be written in terms of the extinction, α :

$$\tau(r, \lambda) = \int_{r_0}^r \alpha(r, \lambda) dr \quad (2.2)$$

As we could see, we only have one equation with two unknown factors, $\beta(r, \lambda)$ and $\tau(r, \lambda)$, so approximations should be done. Furthermore, these unknowns could depend not only on the distance but also on the wavelength

Advantages of using a Raman LIDAR is that elastic LIDARs could have up to a 20% systematic error when determining extinction, while a mechanism like ours diminish it. We dispose the tools to break the degeneration between $\beta(r, \lambda)$ and $\tau(r, \lambda)$ and even reduce systematics due to the wavelength dependence. However, a problem of using Raman LIDAR is that backscatter cross section is approximately four orders of magnitude smaller than Rayleigh one.

Chapter 3

The IFAE LIDAR

Any LIDAR has basically three main components: a collecting surface, a laser and a photodetector element.

The telescope is one of the old CLUE units from HEGRA (High Energy Gamma Ray Astronomy) experiment, an observatory which studied high energy gamma radiation and was operative at La Palma between 1987 and 2002 [2]. CLUE, specifically, was an array of cosmic ray detectors that were set to analyze Cherenkov light emitted by hadronic showers. Each of these units consists of a container that was mechanized such that they can be opened in two shells. Inside, a 1.8 m diameter telescope is installed which, once the container opens, can be pointed into anywhere in the sky (see Figure 3.1). Both the telescope and the container can be controlled remotely. Two of these units have been acquired by IFAE in order to work as a LIDAR and they consist of a container which has its own control system and a telescope placed inside of it. One of them is at IFAE, being already converted to a Raman LIDAR and is thought to be a prototype to optimize the design and to understand the best operation point. Once the design is proven to be ready to work, a clone will be built using the other container, which is located in El Roque de los Muchachos in La Palma with the aim to test its capabilities when operating together with a real Cherenkov telescope, MAGIC. The final goal would be to use them in CTA.

The collecting area is a single parabolic mirror with a diameter and a focal distance both of 1.8m ($f/D=1$), hence, having an aperture of 26.6 deg. The mirror was made with a 6 mm thick float glass with a particularly smooth surface and was coated by Osservatorio Astrofisico of the University of Padova with a layer of aluminum of 50nm thickness. This mirror, which has a hole of 5.5 cm of diameter in its center, is on top of an altazimuthal mount. The remote control was obsoleted and a new one had to be designed and built. This task has been done by the engineer team at IFAE and the remote control is already installed and working. Its reflectivity and PSF were measured when it was built, but new description will be done by us because

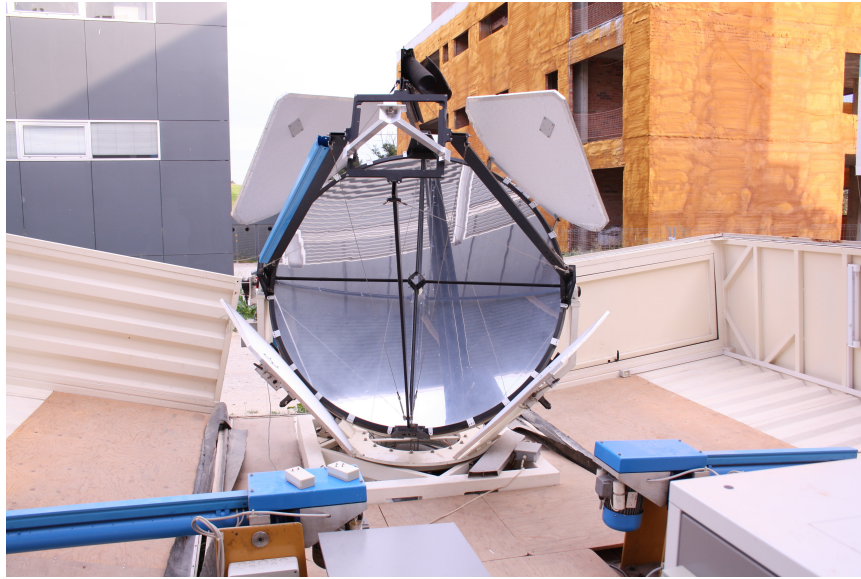


Figure 3.1: Clue container and telescope

its values could have changed due to aging, what provokes that quality of the mirror has decreased and, so, these parameters could not be the same. Moreover, the PSF of this mirror was measured by pointing the telescope to a source at 90 deg zenithal angle obtaining a 5.8 mm PSF while what we want to do is to characterize it at 0° , 30° and 45° zenithal angle, more normal angle for observations with Cherenkov telescopes-

Exclusivity of this instrument is that, although other Raman LIDAR are operating into some observatories like Pierre Auger [5], no one would have such a long-range as ours, being our goal that it could reach 10 km of altitude, where Cherenkov radiation due to electromagnetic showers are produce. Anyway, there's no Raman LIDAR with a collecting area as big as ours.

Atmospheric measurements will be done with a Brilliant Nd-YAG 1064nm laser developed by Quantel (see Figure 3.2). This laser has a compact lightweight housing and offers remarkable performance in terms of energy (short and long-term stabilities) and outstanding beam quality. Its active temperature stabilizator, complete computer control and dust free housing make integration quite easy.

The laser also can be fitted with second and third harmonic generators at 532nm and 355nm, respectively. The emitted pulses would have energies of 360mJ/p, 100mJ/p and 100 mJ/p for each of the wavelengths already mentioned. Thanks to that, we could detect the Raman measurement for N_2 (387 nm and 607 nm) and water vapor H_2O (407 nm) which are the wave-

lengths of our main interest because the peak emission of Cherenkov light is located at 350nm. The laser will emit 5ns pulses with a 20Hz frequency and the beam divergence would be 0.5mrad.



Figure 3.2: Brilliant Nd-YAG 1024nm laser acquired by IFAE with second and third harmonic generators at 532 nm and 355 nm respectively.

To study each of this wavelengths, a detector based on modular optics is being developed, so we will be able to study the wavelengths of our interest separately. It will be formed by different modules and each of them will contain dichroic mirrors and filters specific for a certain wavelength, so they will work as individual one-wavelength detectors their selves: one for N_2 Raman, another for H_2O Raman... Modular optics is being used so modules can be added or removed depending of our interests. After the filters, there will be placed the photomultipliers and the readout electronics.

The laser will be placed on the side of structure which supports the mirror so a biaxial configuration could be considered. But we can insert two flat mirrors in the way they would deviate the laser beam as it it would be going out from the center of the collecting area. Backscattered light will only be collected by the LIDAR once the laser enters the FoV of the telescope. Depending on the biaxiality, the distance when the geometric overlapping starts will change, being basically zero meters for a coaxial configuration. The latter set-up is technically more challenging but being able of measuring the optical depth τ on the first tens of meters could be crucial. Being the IFAE LIDAR a prototype, we decided to go for a coaxial configuration.

Afterwards, the energy must be transported from the focal plane to the

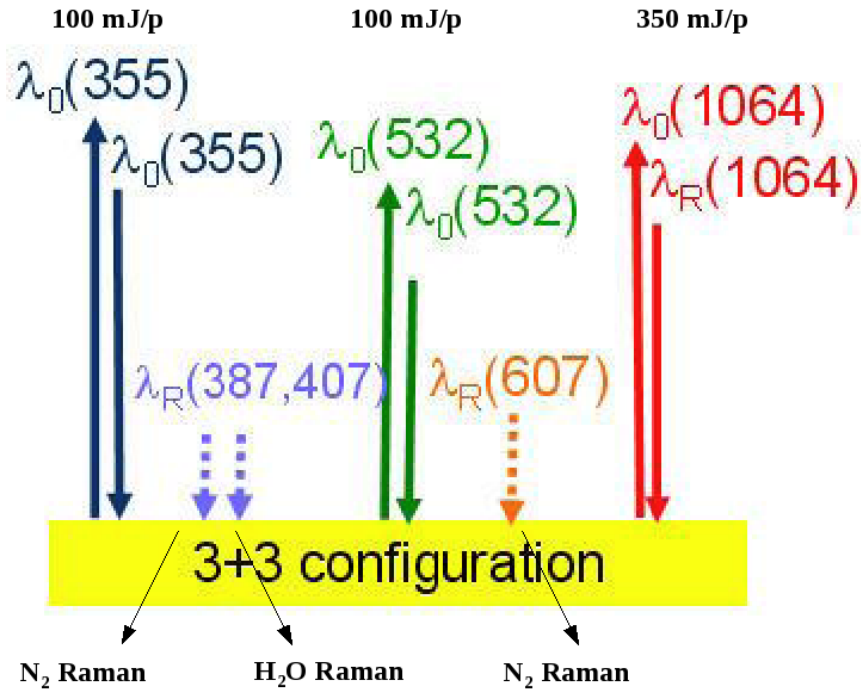


Figure 3.3: Laser emitted wavelengths (355nm, 532nm, 1064nm) and dispersed backscattered Rayleigh and Raman wavelengths for nitrogen (387nm, 607nm) and water vapor (407nm)

detector. Two different set-ups could be considered:

1. Insertion of a convex secondary mirror in the focal plane to convert the system into a Cassegrain mount (see right panel of Figure 3.4), which would make use of the already existent hole in the mirror. This is a typical configuration in optical telescopes. An extremely good alignment and calibration of the two mirrors (primary and secondary) is needed not to lose the spot. Moreover, the CLUE mirror was never designed to have the quality requested by optical telescopes. Both, for the CLUE purpose as well as the LIDAR application, something closer to a light collector than a mirror for optical telescopes is enough. This translates on a PSF of about 6 mm, which becomes critical in a secondary optics due to the magnification. The image of the PSF in the final focal plane would be 6 mm times the f/D relation of the system. Since the hole in the mirror has only 5.5 cm diameter, this would require a secondary quite far from the focal plane and, hence quite large. This makes the secondary configuration costly and challenging from mechanical point of view. It does not seem to be the best option.

- Place the detector in the focal plane and use an optic fiber to guide the received light, as seen on the left of Figure 3.4. It would not increase the PSF and, as the diameter of the fiber could be greater than the PSF, it would collect most of the light. The main problem of this configuration could be radiation losses inside the fiber.

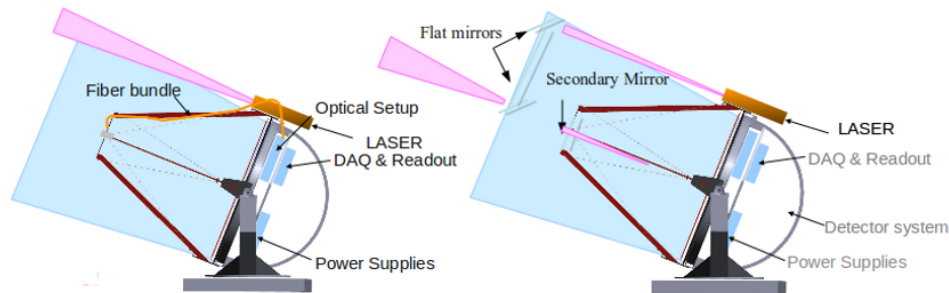


Figure 3.4: Left: Biaxial set-up with a fiber bundle/liquid light guide to collect the radiation . Right: Coaxial configuration with a secondary mirror to set up a Cassegrain

There is one nice solution to reduce possible light losses inside the fiber when transmitting from focal plane, that is to use liquid light guides, a new kind of optical fibers instead of a fiber bundle of quartz fibers. A deep research about this new technology has been done and we feel confident as they have been being used in many different fields as forensics⁴ or particle physics [3], showing excellent responses. They are suitable for our assembly as they are characterized for having high transmittivity, around 80% per every two meters in UV (region of our interest), much bigger than conventional optical quartz fibers (between 40% and 50% per every two meters in the UV range). As they are filled with liquids, they present better flexibility so they're more easy to operate and they have a great aperture angle, what favors transmission and what it is needed in our system due to the f/D focal relation of the telescope. They don't transmit pictures but light, although this is not a problem for us, because we not do imaging but photon counting.

Our main worry was their lifetime, that it is supposed to be around 3 years or 4000 operative hours in general, due to liquid degradation because of the formation of bubbles inside of them. But checking different kind of liquid light guides and trademarks, we have concluded that using *LUMATEC Liquid light guides Series 300* the aging would not be a problem under several

⁴<http://www.rcmp-grc.gc.ca/fsis-ssji/firs-srij/bulletins/forensic-light-source-lumineuse-judiciaire-eng.htm>

conditions. There are many parameters that have influence in the lifetime and stability of the light guide. To assure a long lifetime, light guides should not be exposed to radiation below 320 nm or above 650 nm: shorter wavelengths may destroy the transmission property of the liquid and longer may overheat it and cause bubbles. Under temperatures between -5°C and 35°C there is no degradation of the transmission to be expected, and temperatures over 35°C and below 50°C should not be a problem for a period of a few days. Exceeding these limits do not destroy the liquid itself but the sealing, so bubble may occur. In order to carry out this specifications, we could only use laser's second and third harmonic because the first harmonic, whose wavelength is 1024 nm, exceeds the limit. This is not a problem for us since we are interested in the UV range. We would also need a cooling system to provide temperature stability. With this requirements, liquid light guides transmission properties would be stable over the years. We will use a 3.2 m guide of LUMATEC Series 300, which will allow us to go from the focal plane to the location of the optical detector behind the telescope structure. As liquid light guides has a transmittivity of 80% per every 2 meters, the transmission for our fiber would be around 70% with 8mm nucleus. These light guides are available with a 8 mm active nucleus, which will permit us to collect most of the light reaching the focal plane. We conclude this is the best solution for our system.

So, once studied advantages and inconvenients from all configurations, it will be chosen the use of a single primary mirror with a coaxial set-up and a liquid light guide to transmit the received radiation from the focal plane to the detector system.

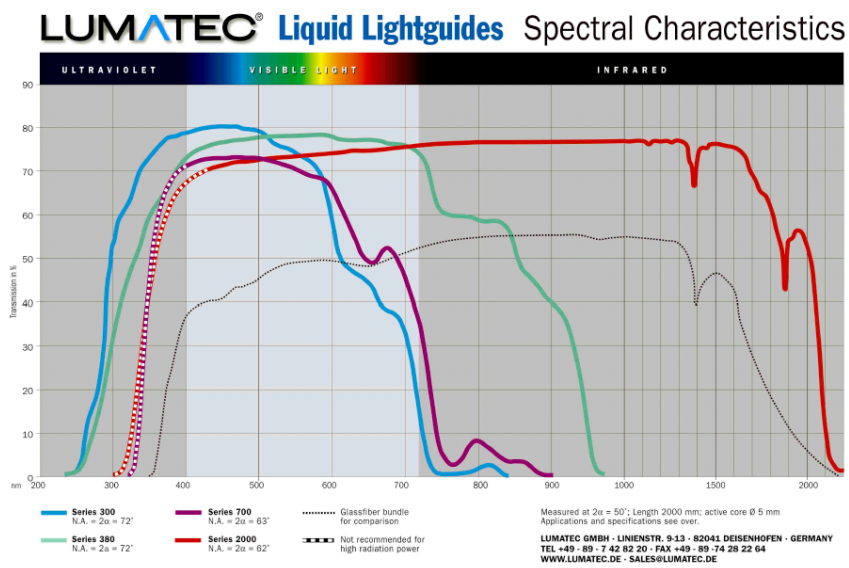


Figure 3.5: Transmission values for LUMATEC liquid light guides. The one of our interest is Series 300, which has a high transmittivity in the whole UV range, up to 80% per every 2 meters. Figure obtained from: http://www.lumatec.de/e_lightguides/e_lightguides.htm

Chapter 4

Reflectivity

One important measurement to portray completely the system, as mentioned in previous chapters, is the determination of the superficial and focused reflectivity of the mirror. In this section, measurements will be shown.

4.1 Superficial Reflectivity

First we want to know the superficial reflectivity of our mirror as a function of wavelength. This is important to understand the effective collection area for each of the recorded wavelength. Moreover, due to aging and a lack of care for the last years (the telescope has been stored since it stopped working for HEGRA experiment), the mirror have some a bit damaged areas and it is cover by a thick layer of dust so its capacity of reflect the light could have decreased. Because of that, we need to make local measurements of the reflectivity in different positions of the mirror to know if it is suitable for the task it is commission for or if an aluminization is needed.

Measurements of local reflectivity on the mirror surface have been done in collaboration with UAB (Universitat Autònoma de Barcelona). We used an AvaLight-DH-S-BAL Deuterium-Halogen Light Source combined with AvaSpec-2048-USB2-SPU-AF Spectrometer and a reference mirror that has already been calibrated by Avantes Company and whose response is provided. The equipment is shown in Figure 4.1 The halogen light is used for our measurements.

The source is connected to the spectrometer thanks to an optical fiber bundle which transmit the light from the first one until the piece that we want to characterize and then collects the reflected light and guides it into the spectrometer. The spectrum is then send to a computer where we can plot the reflectivity in terms on the wavelength. Before trying to measure our LIDAR's mirror reflectivity, it is necessary to obtain the spectrum of the reference tile and substract the dark, in order to have a good and real calibration. This device has to be treated carefully, not only because the

fiber has a minimum bending radius which, if exceeded, could be damaged, but also because the transmission varies appreciably if moving the bundle, so and static configuration should be set.

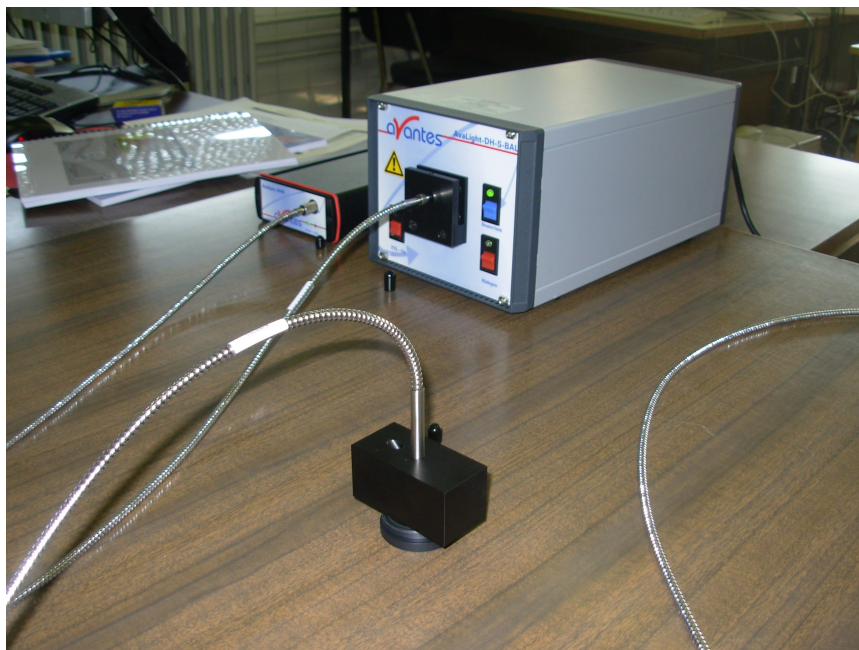


Figure 4.1: Avantes equipment used to measure local reflectivity. On the right is the light source and, next to it, the spectrometer. They are connected by a optical fiber which is plugged in the reference tile, in the front.

First, measurements on the mirror as it was acquired were done. As it had lot of dust on it, reflection was very low, less than 50% in the UV, the area of our main interest. So, a cleaning was needed.

Our mirror do not work as an imaging telescope, but as a light collector, and was not developed neither needs to have the optical quality of optical telescopes. Because of this, there is no reason to think about doing a professional cleaning, as we are only interested in collecting large amounts of light.

First we tentatively tried with a water-cleaning and the reflectivity values already increased by 13% approximately, i.e, reaching 53% at 350nm, but this value is still far from the typical reflectivity of an aluminum coated mirror at that wavelength (which is around 90%). It was visible by eye that dust was still stacked one the mirror.

Therefore, a soap and water cleaning was performed. To get better results, this procedure has been repeated several times, until no improvement was visible. The best results were obtained with this method where the re-

flectivity arised up to 80% in the UV region, a 27% more than only-water cleaning. It is worth noticing that once the mirror has been cleaned at this level, a water-cleaning from time to time is enough to keep it clean.

Twenty four different measurements, twelve positions gauged twice, around all the mirror were done. Although we tried to measure exactly at same points for the second time, it was not very accurate. The twenty four measurements show a dispersion of about 10%. Part of this dispersion could come from systematic errors. From the two measurements in similar positions, an estimation of around 5% maximum systematics uncertainty is done. The additional dispersion is not surprising since, already by visual inspection, one can see that some regions are much more damaged than others.

Plots of all positions and the profile could be checked at Figure 4.2 and Figure 4.3 respectively. It is worth mentioned that the profile is well preserved, so all positions present approximately the same behavior in terms of the wavelength, with an uncertainty smaller than 0.5% for the ultraviolet range which increases until 1% for larger values. This shape curve rise significantly from 60% up to 87% in the UV and until 450 nm, where remains constant for the whole visible spectrum (around a 90% reflected light). So, it responses satisfactorily to the incident light. The value of the reflectivity at 350 nm, wavelength of the peak emission for Cherenkov light, is around 80% of the incoming radiation, which is good enough not to think about doing an aluminization of the mirror. With these results, we can first conclude that our mirror is suitable for the task that is being designed for.

It is worth to point out the collaboration between IFAE and LPTA group in Montpellier, institutions which has a close and official deal to exchange ideas and resources to develop a Raman LIDAR for CTA observatory. This French group has also bought a CLUE unit to construct a Raman LIDAR with it. They have also made superficial reflectivity measurements of the mirror with the equipment borrowed from us. They cleaned its mirror first with water and later with an special gel. This gel does not improve noticeably the reflectivity. So we conclude that there is not need to make another kind of cleaning in our mirror.

4.2 Focused Reflectivity

Another important task is to know the focused reflectivity of the mirror, this is, how the mirror reflects the light as a whole and projects it into the focal plane. This is a very important parameter in the performance of every telescope, because it plays a main role on the absolute scale of collected light. As far as we know, it was never characterized for the HEGRA experiment. We will determine it since the focused reflectivity is a clue of the optical quality of the mirror and it will allow us to fully conclude if the mirror that

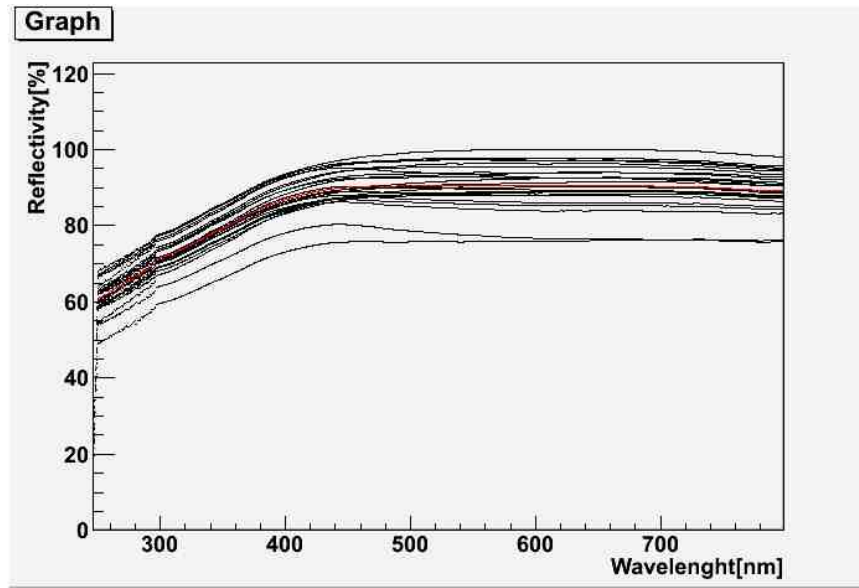


Figure 4.2: Plot of the positions measured on the mirror. The reflectivity is different depending on the point.

we are using is suitable or not to develop a Raman LIDAR with the specified features.

As discussed in the previous section, the reflectivity and quality of the mirror could have diminished due to aging and dust deposit on the mirror surface. That is the reason why we want to characterize it again.

4.2.1 Methodology

While it is quite easy to measure the local reflectivity of a mirror, it is not so straightforward to measure the amount of light that it is focused into a spot of light. That is why we have designed an experiment: focalize the solar light in the focal plane where a metallic piece would be placed. Studying how the temperature varies as function of time we could know how much flux has been reflected by the mirror. This mount is shown on Figure 4.8

The incident solar flux is known by the solar constant, which is the amount of incoming solar electromagnetic radiation per unit area that would be incident on a plane perpendicular to the rays, at a distance of one astronomical unit and it includes all wavelengths of solar electromagnetic radiation, not just the visible light, so it is integrated in the whole energy range. Its value does not remain constant, although it is around 1365 W/m^2 at top atmosphere. Its variation depends basically of the ecliptical position of the Earth, terrestrial latitude and the state of the atmosphere, that is, the

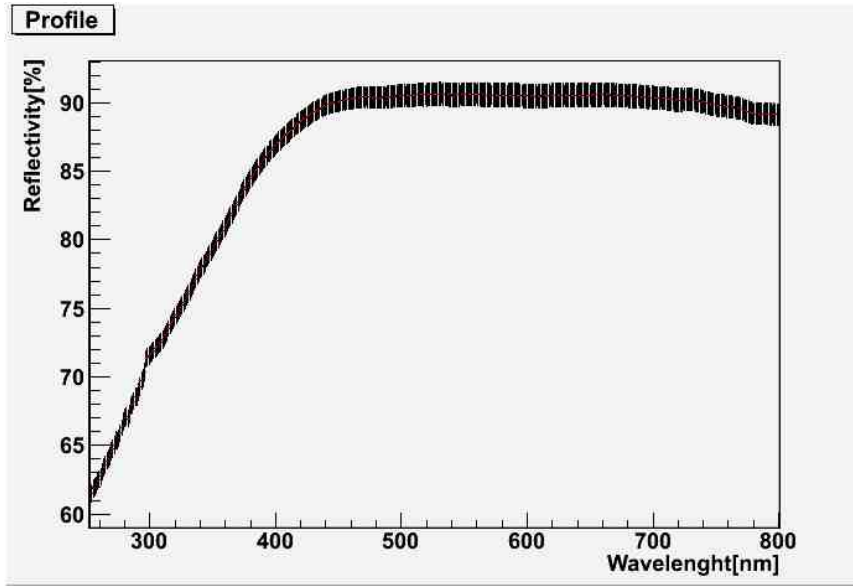


Figure 4.3: Profile of all measurements.

weather conditions. The insolation, that is, the solar radiation striking the surface at certain latitude, could be calculated as:

$$I = S \cos Z \quad (4.1)$$

Where $S \approx 1000 \text{ W/m}^2$ is a clear day solar insolation on a surface perpendicular to incoming solar radiation (this value actually varies greatly due to atmospheric variables) and Z is the zenith angle, which is dependent upon latitude, solar declination angle and time of the day:

$$Z = \cos^{-1}(\sin \phi \sin \delta + \cos \phi \cos \delta \cos H) \quad (4.2)$$

IFAE is at a latitude of $\delta = 41^\circ 30' 3.96''$ and solar declination for summer's solstice is $\delta = 23.5^\circ$. Considering that we want to know the solar radiation at noon, when the Sun is at its culmination, the hour angle H would be $H = 0^\circ$. With all these considerations, we obtain that the insolation would be around 999.8 W/m^2 . As we are calculating it for summer's solstice, when the Sun reaches its maximum declination, this value would set an upper limit for I .

This incident flux can be measured by using a digital light meter, which provides the illuminance (intensity of the amount of visible light) in terms of lux, that is the analogous of the radiometric unit watts per square meter, but with the power at each wavelength weighted according to the luminosity function, a standardized model of human visual brightness perception. As

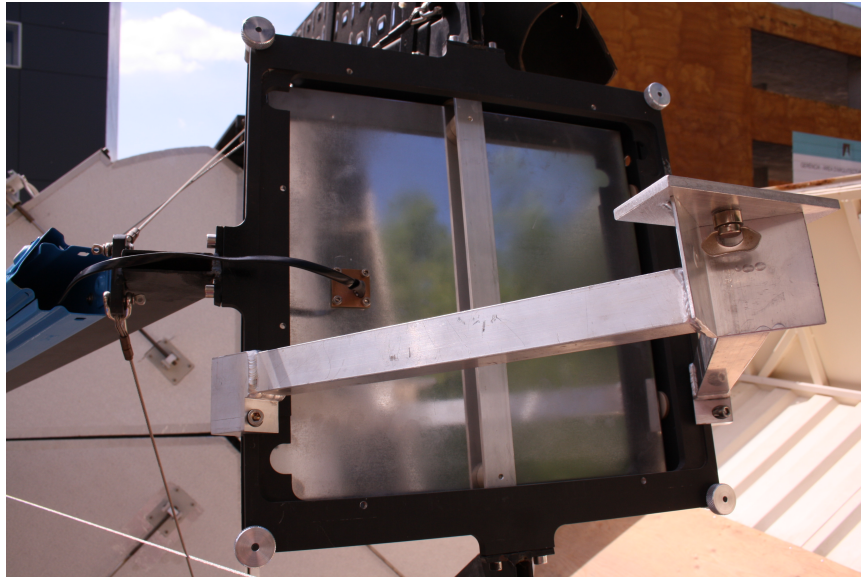


Figure 4.4: Metallic piece placed at focal plane of our telescope and temperature sensor

a reference, bright sunlight provides illuminance of approximately 100,000 lux at Earth's surface. As a first approximation, the light meter was used to check the conditions of the atmosphere when the measurement was done. The luxometer was indicating about 100000 lux, which will be interpreted as having a perfectly clean atmosphere. It is planned to calibrate this light meter with a pyranometer from a meteorological station, which may reduce the small systematic coming from the previous assumption.

The relation between flux and temperature:

$$flux = \frac{Q}{At} = \frac{cm\Delta T}{At} \quad (4.3)$$

where c [J/Kg/K] is the specific heat of the material, m is the mass, ΔT is the change in temperature, A is the area of the telescope and t is integration time. As we are using temperature sensors to know the variation of this parameter, the ΔT factor would be defined in terms of the maximum temperature allowed by the sensor not to break.

It is also important that the temperature extends in the piece of metal as fast as possible placed in the focal plane, so the material must have high thermal conductivity to provide homogenization in temperature in the sample:

$$J = k \left(\frac{\partial T}{\partial s} \right) \quad (4.4)$$

where k [W/K/m] is the thermal conductivity. In terms of heat, this last equation could be written as:

$$Q = \frac{k(T_A - T_B)}{d} At \quad (4.5)$$

$(T_A - T_B)$ is the temperature difference between the incident point of the focused Sun light and the temperature sensor, while d is the distance between these two points.

Looking at these equations, and realizing that we do not want to place too much weight on the focal plane, it seems that we need a metal with a high specific heat and low density (to assure good flux caption and low weight) and a high thermal conductivity so no big temperature gradients would be present at the sample. Also, integration time is important, as it must be much bigger than the time that petals of the telescope need to be completely open (around 40 secs), as we need to point the Sun and, then, open the petals to start collecting light, for security reasons.

With these considerations on mind, calculations have been done to check which metal is the most suitable for our experiment

Material	c [J/kg/K]	Mass [Kg]	Thermal Cond [W/K/m]
Steel	460	13.2	51
Aluminium	880	6.9	209.3
Copper	390	15.56	375
Tin	230	26.39	64
Iron	450	13.49	80.2

Figure 4.5: Different metals considered with their specific heat, thermal conductivity and mass. This last one, has been calculated using Equation (4.1) for a fixed integration time and difference of temperature, supposing a reflected flux of 60% of solar constant just to have a reference of the weight that would be at the focal plane

Several metals were taken in consideration (see Figure 4.8). Comparing all the values, we have decided to use aluminum to construct the metallic piece for the experiment. Finally, a sheet of 4.669 Kg and 340 x340 x14.96 mm dimension has been developed. This metallic piece has an approximate composition of 92% aluminum and 8% of other elements ($\approx 4\%$ magnesium, $\approx 0.4\%$ silicon, $\approx 0.4\%$ iron, ...) With this conditions, and estimating that our mirror would reflect 60% of the incoming flux, we can integrate up to 200 secs without exceeding the restriction imposed by the temperature sensor.

4.2.2 Results

Experiment was done on 28th June with perfect weather conditions. The metallic sheet was placed at the focal plane, where a temperature sensor was fixed at 11 cm from the center. The idea was to point the Sun first producing its image where the sensor was, in order to study how quick the temperature increased as a function of time. Then, we would repeat the procedure by focusing sunlight at the center, what would provide us information about the heat dispersion in terms of thermal conductivity, which provokes that temperature gradients exist.

First, the telescope was pointed to the Sun, which was focused on the sensor. Then, due to security reasons, petals were open. At this point, the temperature started to increase with a non prominent slope. Once the petals of the mirror were completely opened, a fast increase of temperature was appreciable, as we can check on Figure 4.6. Then, the sensor reached its maximum, so the graphic saturates, although temperature should keep increasing. After, we start closing the petals, causing a descent of the temperature, captured as a prominent descent in the graphics favored by the presence of wind. Then, the petals remained closed and temperature kept decreasing.

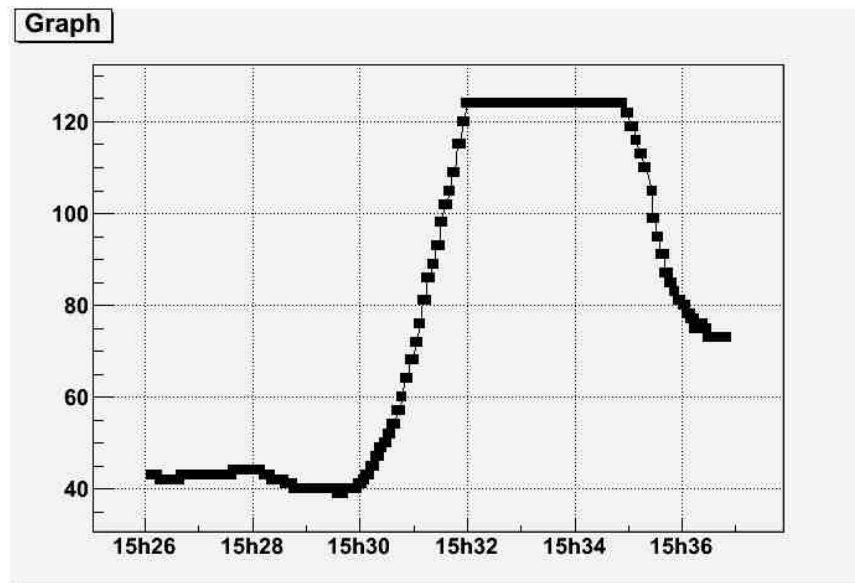


Figure 4.6: Increase of temperature as function of time while focusing the Sun into the sensor. Prominent rise of temperature is visible when petals are completely open and diffusion drop is seen when these are closed. Different phases are indicated.

Then, after allowing the temperature to stabilize, the same procedure

was followed but focusing on the center of the sheet. Result is shown on Figure 4.7. This time, the temperature did not rise up as fast as before because the heat takes some time to propagate from the center to where the sensor is placed. In this case, a cloud appeared in front of the Sun and there was a decline on the flux captured by our mirror. When that happened, we decided to close the petals and stop doing measurements.

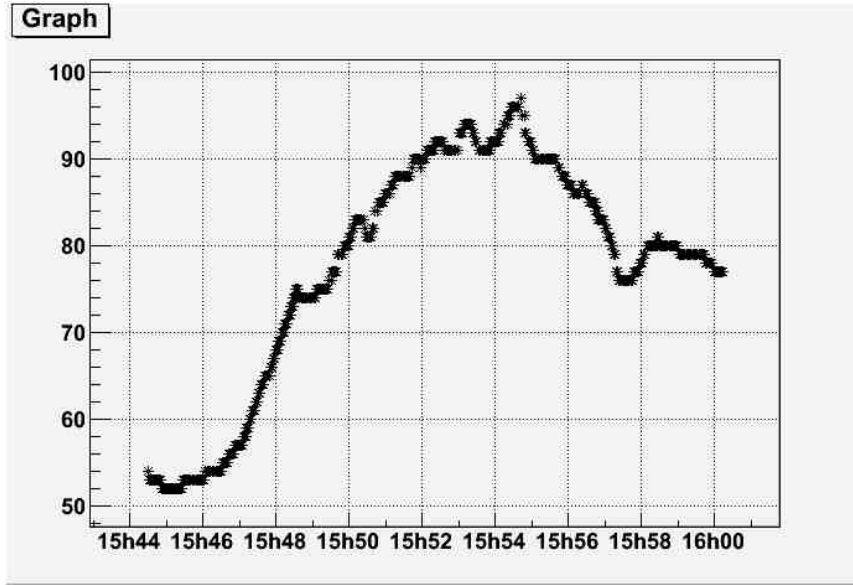


Figure 4.7: Temperature variation as a result of the focus at the center of the metallic piece. The increase is much slower, due to the dispersion of heat, which depends on the thermal conductivity. Phases are visible.

Now, we want to calculate the amount of flux reflected by our telescope and detected by our metallic sheet. Cheking the increase of temperature from the point that the petals were opened until the saturation of the sensor, we can see that $\Delta T = 70^{\circ}C$ in 83 seconds, when the Sun was focused on the sensor (Figure 4.6). Similarly, one can also get $\frac{\Delta T}{\Delta t}$ when it is focused 11 cm away from the sensor (Figure 4.7). Then, considering an exponential falling for the temperature in terms of the position as:

$$\left(\frac{\Delta T}{\Delta t}\right) = k \exp(-\alpha r) \quad (4.6)$$

we can determine de slope in terms of the position:

$$\left(\frac{\Delta T}{\Delta t}\right) (r) = \left(\frac{\Delta T}{\Delta t}\right)_{sensor} \exp - \left\{ \left(\ln \left(\frac{\left(\frac{\Delta T}{\Delta t}\right)_{sensor}}{\left(\frac{\Delta T}{\Delta t}\right)_{center}} \right) \right) \left(\frac{r}{d} \right) \right\} \quad (4.7)$$

The flux stored by the aluminum sheet is given by $\frac{\Delta T}{\Delta t}$ at each point of the sheet ($(\frac{\Delta T}{\Delta t})_{sensor} = (\frac{70}{83}), (\frac{\Delta T}{\Delta t})_{center} = (\frac{19}{108})$). To compute that, we use equation 4.3, which can also be written as:

$$flux_{stored} = \int \frac{(\frac{\Delta T}{\Delta t}) c \rho \delta(V)}{A} = c \rho h \int_{x_2}^{x_1} \int_{y_2}^{y_1} \left(\frac{\Delta T}{\Delta t}\right) (r) dx dy \quad (4.8)$$

in this equation, c is the specific heat, $\rho = 2700 Kg/m^3$ is the aluminum density, h is the thickness of the sheet and the limits of the integrals are the dimensions of the sheet measured from the sensor position.

Although we know the slope at the sensor $(\frac{\Delta T}{\Delta t})_{sensor} = (\frac{70}{83})$ and at the center $(\frac{\Delta T}{\Delta t})_{center} = (\frac{19}{108})$, we should extrapolate along the sheet. As first approximation, the temperature gradient as function of time could be calculated as:

$$\left(\frac{\Delta T}{\Delta t}\right) = \left(\frac{\Delta T}{\Delta t}\right)_{sensor} - \left\{ \left(\frac{\Delta T}{\Delta t}\right)_{sensor} - \left(\frac{\Delta T}{\Delta t}\right)_{center} \right\} \left(\frac{r}{d}\right) \quad (4.9)$$

where d is the sensor-center distance and r is the position in the sheet, defined in cartesian coordinates as $\sqrt{x^2 + y^2}$. With this, and considering an exponential falling for the temperature in terms of the position as:

Using 4.7 and integrating, we compute the stored flux:

$$flux_{stored} \approx 215W/m^2 \quad (4.10)$$

This is not the total flux focused to the metallic sheet. While the focused Sun is providing heat to the system, there are also losses due to radiation to the environment. This radiated flux can be obtained by measuring the negative slope which appears after the petals of the telescope get closed. In this case, temperature varies 11 ° C in 64 seconds and 19 ° C in 108 seconds respectively, giving approximately the same value. So, the radiated flux is:

$$flux_{radiated} \approx 280W/m^2 \quad (4.11)$$

So, the total amount of flux dispersed from the metallic sheet is:

$$flux_{focused} = flux_{stored} + flux_{radiated} \approx 495W/m^2 \quad (4.12)$$

On the other hand, we could also calculate the solar flux we expect to measure. To do this task, we have weighted the irradiance solar spectrum under the atmosphere with the reflectivity profile of Section 4:

$$\text{flux}_{\text{expected}} = \int R(\lambda)P(\lambda)\delta\lambda \quad (4.13)$$

where $R(\lambda)$ is the reflectivity, $P(\lambda)$ is the spectral power in units $[\text{W}/\text{m}^2/\mu\text{m}]$ and $\delta(\lambda)$ is the wavelength step considered. This equation could be approximated, for small enough $\Delta\lambda$ by:

$$\text{flux}_{\text{expected}} = \Sigma R(\lambda)P(\lambda)\Delta(\lambda) \quad (4.14)$$

Applying this method over the hole wavelength range, we have obtained that the expected flux is:

$$\text{flux}_{\text{expected}} = 625\text{W}/\text{m}^2 \quad (4.15)$$

The ratio between the focused and the expected flux give the correction factor (f) to convert the local reflectivity into focal:

$$\left(\frac{\text{flux}_{\text{focused}}}{\text{flux}_{\text{expected}}} \right) = 0.79 \quad (4.16)$$

The reduction of the focal reflectivity is, in principle, a geometric effect due to the mirror imperfections. Hence, one can safely assume that there is no dependence on the wavelength. Under this assumption, the local reflectivity shown in Figure 4.3 can be translated into focal just by multiplying by the factor $f = 0.79$. This lead to a reflectivity of $\approx 64\%$ at 350 nm, where the peak of the Cherenkov light is.

Chapter 5

Point Spread Function

The Point Spread Function (PSF) describes the response of an imaging system to a point source and it can be interpreted as the irradiance distribution of that point. In functional terms it is the spatial domain version of the modulation transfer function.

Although we observe point-like sources, the image not necessarily would be a point. This is due to aberrations and diffraction in the optical system, which will spread the image over a finite area.

The PSF was measured when the mirror was made for the HEGRA experiment. About 80% of the light was collected in a 6 mm side square. To calculate the CLUE mirror optical quality, the telescope was illuminated with a 600W halogen lamp place at a distance of 90 meters at 90 deg zenithal angle, what produced a PSF of 6 mm approximately, as mentioned before. The results are shown in Figure 5.1 for several of the CLUE mirrors.

It is true that we are working with a light collector, not an imaging telescope, so we do not worry to much about having very high image quality but about having a large area to collect large amounts of light. But even with this property, we do not expect a PSF too big because, despite is not a big deal for us, it also affects our data, because it would lead to have more background light and less radiation inside the fiber.

As the mirror is now much older and dust has been deposited on its surface, optical quality has probably decreased and the PSF may have increased its value. We need to characterize it not only to portray our mirror but also because we have to know the size of the spot so most of the light could be collected by the liquid light guide. As well, as seen on Figure 5.1, the point spread function was obtain for several CLUE mirrors and the percentage of light varies from one to another. As we do not know which one is ours, we need to characterize it. These are the reasons why we want to measure it again.

Our procedure would be different from that taken by the CLUE team. We would use some bright stars instead of an halogen lamp to study their

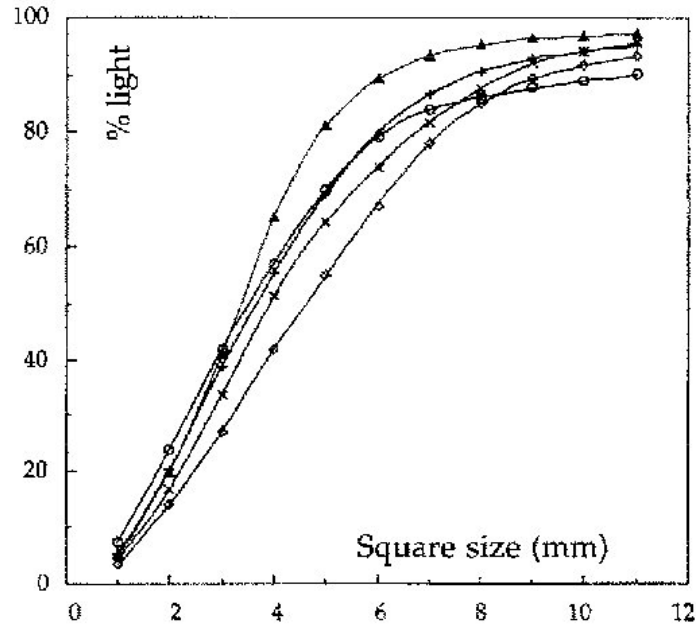


Figure 5.1: Percentage of reflected light falling within a square of given side for five different CLUE mirrors of production series. Image taken from [2]

images, which is also valid as they can be considered point-like sources. This measurements could be done by following α -Boo and α -Lyr at different zenith angles, preferably at 0, 30 and 45 deg. These measurements at various celestial latitudes are thought because the PSF could vary depending of the pointing position of the telescope: as the mirror is not too thick, deviation from the parabolic mirror thanks to gravity action could appear and so the focusing could change as a function of the position. This modifications should be known and characterized. Moreover, angles below 45 degrees are more realistic for the aimed application of the telescope than 90 degrees zenith.

Images will be taken using a Canon EOS 1000D camera placed next to the focal plane of the mirror and they will be studied with IRAF astronomical software, which provides all necessary tools to completely determine the point spread function. Some squares of different sizes were drawn on a transparent piece of paper located at the focal plane to work as reference for the calibration. The packages used to obtain the PSF by adjusting to a gaussian profile were *imexam* and *psfmeasure* [6]

Observations were done on 1st July night. As the container is placed at the University, it is surrounded by many buildings and it is contaminated

by the light coming from the campus. Because to these reasons and the presence of clouds in some regions in the sky, the only bright visible target was Vega (αLyr). It was pictured at approximately between 10° and 30° zenith angle. Pictures of stars a lower zenith angle are quite difficult due to the background light as well as the building of the campus. Having pictures of Vega between 10° and 30° should be enough to understand both if the PSF has degraded and the importance of the zenith angle effect.

The analysis computes a FWHM of 14 pixels, which corresponds to a PSF of 5 mm approximately and does not show any significant difference as a function of zenith angle. Those results are compatible with the value first obtained by the CLUE team people.

Chapter 6

Summary

High energy gamma-ray astronomy is reaching further with the construction of new observatories as CTA would be. The advance in the technology of this third generation telescopes would provide them with an increase of their sensitivity, what would allow to dive deeper into the VHE Universe.

To reduce the systematic uncertainties and increase the duty cycle of the observatory, Raman LIDARs are planned. They would provide information about the vertical distribution of aerosols in the atmosphere and the optical depth for the conditions of the atmosphere when the data would be taken. The use of a Raman LIDAR for Cherenkov telescopes is a challenge. Although LIDARs have been used together with Cherenkov telescopes, they were elastic. Moreover, the distance to which one should be able measure the atmosphere conditions clearly exceed the current world record.

IFAE is developing a prototype Raman LIDAR to understand what is the best configuration to reach the goals with an old CLUE unit together with a laser. Once the best configuration is clear, a clone will be built with another container located at El Roque de los Muchachos to operate together with MAGIC. A coaxial set-up, which is technically more complex but may lead to some advantages, is planned. The newly available liquid light guides seem to be the best option to transport the radiation from the focal plane to the detector units.

The mirror will mainly work as a light collector, not as an imaging telescope. But we need a quite good reflectivity in the wavelength range of interest (about 350 nm) and a reasonable point spread function to collect most of the light with the liquid light fiber. Otherwise, we would lose light limiting the distance up to which the optical depth of the atmosphere can be measured. The reflectivity (superficial and focused) and the PSF has been measured for the CLUE mirror located at IFAE. The optical quality and reflectivity have not decreased significantly during the several years that the container has been storage without any maintenance. The results obtained confirm that the mirror is suitable for the task that is assigned.

Bibliography

- [1] Diehl. RL, “Particle Acceleration in Cosmic Sites”, Eur. Phys. J. D 55, 509 - 518 (2009)
- [2] Alexandreas. D et al, “Status report on CLUE”, Nuclear Instruments and Methods in Physics Research, 1995, Volume 360, 385-389.
- [3] Kawarabayashi. J et al, “Potential on Liquid Light Guide as Distributed Radiation Sensor”, Nuclear Science Symposium Conference Record, 2004, Volume 2, 712-714
- [4] Mussa R. et al, “Atmospheric Monitoring for the Pierre Auger Observatory”, Nuclear Physics B, 2009, Volume 190, 272-277
- [5] Rizi V. et al, “The Use of Raman LIDAR for Atmospheric Monitoring at Pierre Auger Observatory”, GAP, 2002-2004
- [6] Valdes F., “Psfmeasure/Starfocus: IRAF PSF Measuring Tasks”